Synthesis and Characterization of Ag- or Sb-Doped ZnO Nanorods by a Facile Hydrothermal Route

Oleg Lupan,*,†,‡ Lee Chow,†,§ Luis K. Ono,† Beatriz Roldan Cuenya,†,‖ Guangyu Chai,⊥ Hani Khallaf,† Sanghoon Park,† and Alfons Schulte†

Department of Physics, University of Central Florida, P.O. Box 162385, Orlando, Florida 32816, Department of Microelectronics and Semiconductor Devices, Technical University of Moldova, 168 Stefan Cel Mare Boulevard, MD-2004 Chisinau, Republic of Moldova, Advanced Materials Processing and Analysis Center, and Department of Mechanical, Materials, and Aerospace Engineering, University of Central Florida, P.O. Box 162385, Orlando, Florida 32816, Department of Civil, Environmental and Construction Engineering, University of Central Florida, Orlando, Florida, and Apollo Technologies, Inc., 205 Waymont Court, S111, Lake Mary, Florida 32746

ZnO nanorods doped with Ag and Sb have been synthesized by a facile hydrothermal technique. Crystal quality, morphology, chemical/electronic composition, local structure, and vibrational mode properties are investigated by X-ray diffraction (XRD), scanning electron microscopy (SEM), X-ray photoelectron spectroscopy (XPS), and micro-Raman spectroscopy. Evidence of dopant incorporation is demonstrated in the XPS measurements of both Sb-doped and Ag-doped ZnO nanorods. From XRD data, it was found that the doped ZnO nanorods have a lower degree of crystallinity. The lattice constants of doped ZnO nanorods were slightly larger than that of the pure samples.

1. Introduction

Recently, zinc oxide (ZnO) nanorods have been extensively investigated due to their potential for the development of novel nanodevices. Their excellent properties such as a wide band gap (3.37 eV at 300 K), a large exciton binding energy (60 meV), and a large melting point of 1975 °C ensure applications in miniaturized photodetectors,[1,2] light emitting diodes,[3,4] laser light source,[5] and nanosensors[6,7] in harsh environments. For ZnO, addition of impurities often induces dramatic changes in their electrical and optical properties, which suggests new applications.

Usually, undoped ZnO exhibits *n*-type conductivity, which can be ascribed to the asymmetric doping limitations[8] and propensity to defects or impurities.[9,10] *P*-type doping of ZnO films has been achieved using P,[11] N,[12] As,[13] Li,[14] Sb,[15−18] and Ag[19,20] as dopants. These dopants and defect complexes, introduced through synthesis techniques, can define the type of conductivity[21] and optical[22,23] and electrical properties[22,24] of ZnO. A model for a large-sized mismatched group V dopant such as Sb in ZnO was reported in which a $Sb_{Zn}-2V_{Zn}$ complex was thought to be a suitable acceptor instead of a deep Sb_O acceptor.[15,16] Pure Ag- or Sb-doped ZnO has been effectively prepared by pulsed laser deposition,[16,19,26] radio frequency magnetron sputtering,[25,27] and molecular beam epitaxy.[28] Most of the above techniques employ physical means to dope impurities into ZnO, which do not ensure stoichiometric composition. The solution growth method, on the other hand, is a facile, low temperature, and low cost method that can produce high quality and stoichiometric ZnO material.

In this paper, we report an inexpensive, *template-free*, and rapid hydrothermal growth technique to dope ZnO nanorods at low temperatures. We compare the effectiveness of three different characterization techniques on the determination of the impurity incorporation into ZnO nanorods. We found that the effects of Sb and Ag dopants on the structural, chemical, and optical properties and vibrational modes of ZnO nanorods varied. While in X-ray photoelectron spectroscopy (XPS), the signals came directly from the impurities, so it is relatively straightforward to detect the impurity concentration. For X-ray diffraction (XRD) and Raman measurements, the signals came indirectly from the structural and vibrational mode changes due to the impurity incorporation, and therefore it is much more difficult to obtain impurity concentration information using these two methods.

2. Experimental Details

2.1. Synthesis. Slices of *p*-type Si(100) cleaved from a Si wafer were used as substrates for the synthesis of the ZnO nanorods. Before the synthesis process starts, the silicon (Si) substrates were sequentially cleaned with an acetone:ethanol (50:50) mixture in an ultrasonic bath and etched by piranha solution (2:1 mixture of concentrated H_2SO_4/30% H_2O_2) at room temperature for 25 min. Solvent (acetone or isopropylalcohol) was used to remove organic contaminants as reported before.[29,30] After this step, substrates were rinsed with deionized water and then blown dry with a flux of air[29,30] immediately before the hydrothermal process was started.

All the chemical reagents used in our experiments were of analytical grade and used without further purification. In a typical procedure, zinc sulfate heptahydrate [$Zn(SO_4)\cdot 7H_2O$] was first dissolved into 100 mL of deionized (DI) water, and

* Corresponding author. E-mail: lupan@physics.ucf.edu.
† Department of Physics, University of Central Florida.
‡ Department of Microelectronics and Semiconductor Devices, Technical University of Moldova.
§ Advanced Materials Processing and Analysis Center, and Department of Mechanical, Materials, and Aerospace Engineering, University of Central Florida.
‖ Department of Civil, Environmental and Construction Engineering, University of Central Florida.
⊥ Apollo Technologies, Inc.

then 50 mL of ammonia (NH_4OH) (29.32%, Fisher Scientific) was added and stirred for 10 min to mix completely at room temperature. The first set of pure ZnO nanorod (#1) samples was synthesized using 0.1–0.5 M $Zn(SO_4) \cdot 7H_2O$. The second set of samples (#2) was prepared using 0.1–0.5 M zinc sulfate and 0.001–0.005 M antimony chloride ($SbCl_3$) (99.7%) which was dissolved in 100 mL of DI water plus 3 mL of HCl. Another set of samples (#3) was prepared using 0.1–0.5 M $Zn(SO_4) \cdot 7H_2O$ and 0.001–0.005 M silver nitrate $Ag(NO_3)$ (99.7%), which was dissolved in 100 mL of DI water. An ammonia solution (29.6%) was added until the solution became transparent and clear, which immediately started a heterogeneous reaction.

Subsequently, the resulting aqueous solution was poured into a 120 mL reactor (75% filled). The vessels were placed on a preheated oven for 10 and 20 min at 95 °C and then allowed to cool to room temperature in 30 min. After the reaction was completed, the grown ZnO nanorods on the substrates were rinsed in deionized water for 2 min, and then the samples were dried in air at 150 °C for 5 min. Manipulation and reactions were carried out in air inside a fume hood.

2.2. Characterization. The samples of pure and doped ZnO nanorods were analyzed by X-ray diffraction (XRD) using a Rigaku "DB/MAX" powder diffractometer with a nickel-filtered Cu Kα radiation source ($\lambda = 1.54178$ Å) and a scanning rate of 0.02°/s in the 2θ range from 10 to 90°. Data acquisition was made with the software Data Scan 3.1 and analyzed with Jade 3.1 (from Materials Data, Inc.). The crystal phase was determined from X-ray diffraction patterns. The size and morphology of the samples with ZnO nanorods were observed with a JEOL scanning electron microscope (SEM).

The compositional analysis of ZnO nanorods was carried out using energy-dispersive X-ray spectroscopy (EDX), in combination with SEM. The different characterization techniques confirmed that the nanorods are crystalline with regular rods distributed homogeneously throughout the substrate surface.

Information on vibrational modes in pure and doped ZnO nanorods was obtained from Raman backscattering experiments in a micro-Raman setup Horiba Jobin Yvon LabRam IR spectrometer with a charge-coupled detector (CCD). This system has a spatial resolution of 2 μm. Raman spectra were excited with 1.96 eV photons from a Helium Neon laser ($\lambda \sim 633$ nm) with less than 4 mW of power at the sample. The spectral resolution was better than 2 cm^{-1}, and the instrument was calibrated using a naphthalene standard.

For X-ray photoemission spectroscopy (XPS), the ex situ prepared samples were mounted on a molybdenum sample holder and subsequently transferred into a modular ultrahigh vacuum (UHV) system (SPECS GmbH) especially designed for the preparation and characterization of nanoscale materials. The pressure during the X-ray photoelectron spectroscopy (XPS) measurements was $\sim 6 \times 10^{-10}$ mbar. The XPS measurements were conducted in the analysis chamber equipped with a hemispherical electron energy analyzer (Phoibos 100, SPECS GmbH) and a dual-anode (Al Kα, 1486.6 eV, and Ag Lα, 2984.4 eV) monochromatic X-ray source (XR50M, SPECS GmbH). Survey and high-resolution spectra were measured with pass energies of 50 and 18 eV, respectively. The energy resolution of our monochromatic XPS system was calibrated by using a clean Au(111) crystal. For that reference sample, a FWMH of 0.9 eV was obtained. The X-ray spot size in our setup is about 3.5×1 mm^2, and the sample size is ~ 5–$10 \times$ 10 mm^2. For the quantitative analysis of the peak positions and relative spectral areas of the Zn-2p, Sb-4d, Ag-3d, O-1s, and
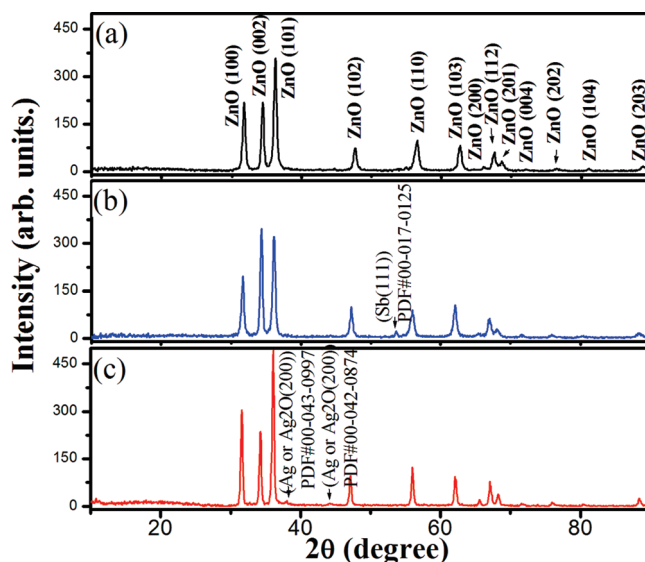

Figure 1. XRD patterns of the ZnO nanorods: (a) undoped, (b) Sb-doped, and (c) Ag-doped.

C-1s components, the raw XPS spectra were fitted with Gaussian–Lorentzian (G–L) functions. The intensity ratios between the 2p$_{3/2}$ and 2p$_{1/2}$ (Zn), 4d$_{5/2}$ and 4d$_{3/2}$ (Sb), and 3d$_{5/2}$ and 3d$_{3/2}$ (Ag) doublets due to spin–orbit coupling were fixed to 2, 1.5, and 1.5, respectively. The concentration of the different dopants relative to ZnO was estimated from the intensity ratios (Sb-4d$_{5/2}$/Zn-2p$_{3/2}$ and Ag-3d$_{5/2}$/Zn-2p$_{3/2}$) after proper normalization using the atomic sensitivity factors (ASF) recommended by the manufacturer of our XPS system (SPECS GmbH).

3. Results and Discussion

3.1. Structural and Morphological Characterization of ZnO Nanorods. Changes of phase structure of the ZnO nanorods were investigated by X-ray diffraction. Figure 1 shows the XRD patterns of pure, Ag- and Sb-doped ZnO nanorods, which demonstrate that all the ZnO nanorods are crystallized in wurtzite structure.[31]

Figure 1a shows the XRD pattern of pure ZnO nanorods recorded in the range of 10–90° with a scanning step of 0.02°. All diffraction peaks can be attributed to crystalline ZnO with the hexagonal wurtzite structure (space group: P6$_3$mc(186); $a = 0.3249$ nm, $c = 0.5206$ nm). The data are in agreement with the Joint Committee on Powder Diffraction Standards (JCPDS) card for ZnO (JCPDS 036-1451).[31] For antimony, in Figure 1(b) an impurity phase was observed at 53.5° (Sb, PDF#00-017-0125). It should be pointed out that a residual phase of silver was found (Figure 1c) in sample #3. No characteristic peaks of impurity phases such as Zn, S, or Zn(OH)$_2$ were observed for Ag- or Sb-doped ZnO (Figure 1), and no diffraction peaks except ZnO were found, which indicates that only single-phase wurtzite ZnO is present. In Figure 1(a), the strongest detected (hkl) peaks are at 2θ values of 31.79°, 34.42°, 36.25°, 47.51°, 56.62°, and 62.83°, corresponding to the following lattice planes: (100), (002), (101), (102), (110), and (103), respectively.

To examine the surface morphology, SEM has been used. Typical SEM images of the ZnO nanorods and an individual one are shown in Figure 2. The overall morphology of the pure ZnO nanorods on the substrate is shown in Figure 2(a), which indicates the obtained products consist of ZnO nanorods with an average radius of 100 nm. The lengths of ZnO nanorods are about 2 μm. The inset in Figure 2a corresponds to a high-
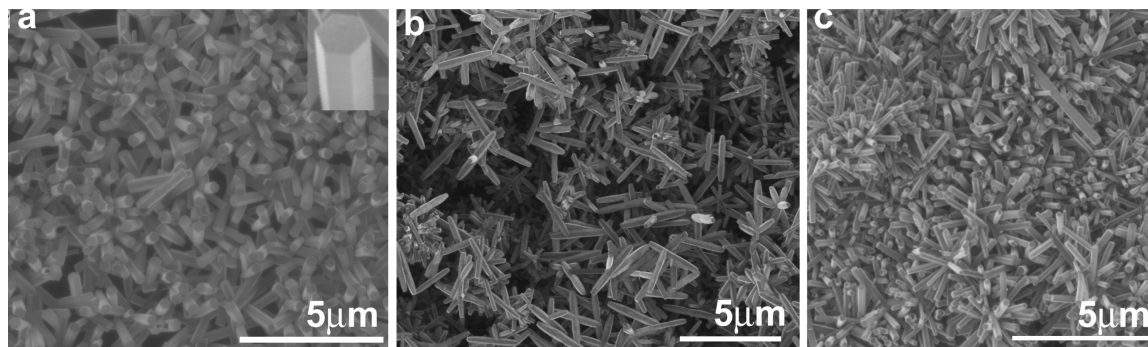
Characterization of Ag- or Sb-Doped ZnO Nanorods

J. Phys. Chem. C, Vol. 114, No. 29, 2010 **12403**

Figure 2. SEM images of ZnO nanorods: (a) pure (the inset is SEM images of a single ZnO nanorod), (b) Sb-doped, and (c) Ag-doped.
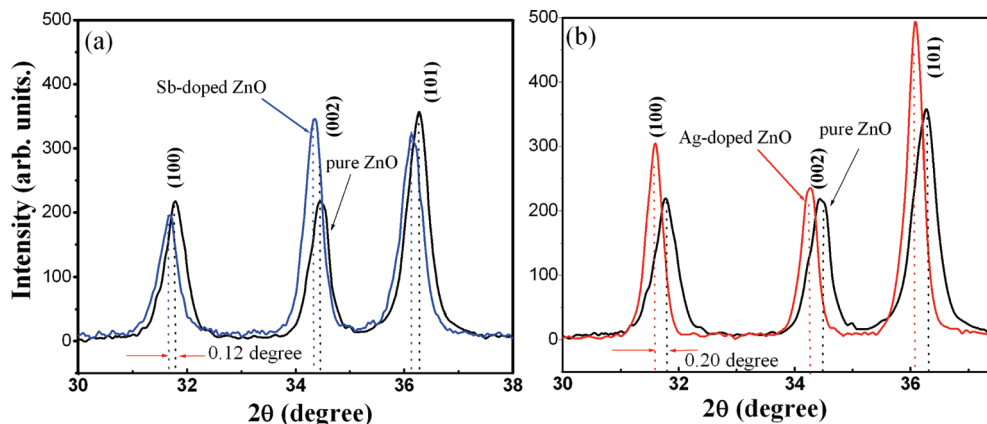

Figure 3. Comparison of (100), (002), and (101) peaks from the XRD pattern of pure ZnO nanorods and ZnO nanorods doped with (a) Sb and (b) Ag.

TABLE 1: Parameters Obtained for the (100), (002), and (101) Diffraction Peaks

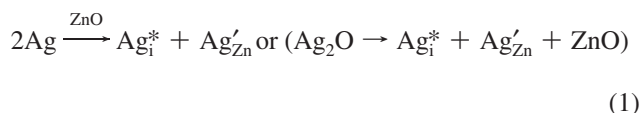| sample	description	(hkl) planes	2θ (deg)	[fwhm] (deg)
#1	ZnO	(100)	31.792	0.408
		(002)	34.423	0.353
		(101)	36.252	0.417
#2	Sb−ZnO	(100)	31.678	0.468
		(002)	34.306	0.417
		(101)	36.114	0.518
#3	Ag−ZnO	(100)	31.595	0.341
		(002)	34.229	0.341
		(101)	36.058	0.377

resolution SEM image taken of a single rod and displays the characteristic hexagonal base of ZnO nanorods. The morphology of the Sb- and Ag-doped ZnO nanorods grown on Si is shown in Figure 2(b) and (c), respectively. According to our experimental results, the nanorods obtained by our process can be easily transferred to another clean substrate and handled by focused ion beam (FIB) fabrication of micronanodevices.[1,6,7] From the SEM images of the doped samples, no significant change of their hexagonal rod morphology was observed.

To study the effect of doping on the crystallinity of the ZnO nanorods, the intensity of the (100), (002), and (101) diffraction peaks was monitored. The intensity of the diffraction peaks (100) and (101) decreased, and their full width at half-maximum (fwhm) increased for Sb-doped samples (see Figure 3a and Table 1). For Ag-doped ZnO samples (see Figure 3b and Table 1), it was observed that there were minute changes in the intensity of the diffraction peaks (100), (002), and (101) and their full width at half-maximum. Such changes in crystallinity might be the result of changes in the atomic environment due to impurity doping on ZnO samples.[32]

The ionic radii of Ag, Sb, and Zn are $r(Ag^{1+}) = 0.126$ nm, $r(Sb^{3+}) = 0.076$ nm, and $r(Zn^{2+}) = 0.074$ nm, respectively.[33,34] A larger lattice deformation was observed for Ag-doped ZnO due to large differences in ionic radii. From the XRD data, we observed a change which indicates the lattice deformation of doped ZnO nanorods. In Figure 3(a), there was a small shift (~0.12°) to a lower 2θ angle value of the XRD diffraction peaks for Sb-doped ZnO nanorods as compared with those of pure ZnO nanorods. No change of the crystalline structure was detected, which suggests that the most Sb atoms were in the ZnO wurtzite lattice. Previously, a Sb dopant in ZnO was predicted to substitute a Zn atom and simultaneously connect two Zn vacancies to form a $Sb_{Zn}-2\,V_{Zn}$ complex, which is a shallow acceptor.[15,18] According to Xiu et al.,[18] the complex $Sb_{Zn}-2V_{Zn}$ could be the explanation of strong p-type conductivity in Sb-doped ZnO films. This result is attributed to a small lattice mismatch between radii of Zn^{2+} (0.074 nm) and Sb^{3+} (0.076 nm), and it indicates that Sb ions systematically substituted Zn ions in the films without deteriorating its crystal structure.[10,36]

In Figure 3(b) there was a 0.20° shift to a lower 2θ angle value of the XRD diffraction peaks for Ag-doped ZnO nanorods as compared with those of pure ZnO nanorods. This is due to the fact that the radius of the Ag^{1+} ion is greater than that of Zn^{2+} which may cause an expansion of the lattice parameter in the Ag-doped ZnO nanorods. The full width at half-maximum and intensity of the peaks was monitored to evaluate the crystal quality of the Ag−ZnO nanorods (see Table 1). The change of fwhm from 0.417 nm (pure ZnO) to 0.377 nm (Ag-doped ZnO) and increase in intensity of the (101) peak are shown in Figure 1(a) and (c). The highest intensities of the XRD peaks were obtained from Ag-doped nanorods. It is possible that heterogeneous nucleation is facilitated in the presence of Ag⁺ ions in

the ZnO structure, which enhances the growth rate in the (101) direction. This suggests that Ag atoms could be incorporated into the lattice of ZnO only as substitution for Zn atom sites.[35] Ag as an amphoteric dopant in ZnO can be in the interstitial sites (Ag_i^*) and on substitutional Zn^{2+} sites[19] (Ag'_{Zn}) expressed by the reaction

$$2Ag \xrightarrow{ZnO} Ag_i^* + Ag'_{Zn} \text{ or } (Ag_2O \rightarrow Ag_i^* + Ag'_{Zn} + ZnO) \tag{1}$$

The lattice constants a and c of wurtzite structure ZnO were calculated, according to Bragg's law[37]

$$n\lambda = 2d \sin\theta \tag{2}$$

where n is the order of diffraction (usually $n = 1$); λ is the X-ray wavelength; and d is the spacing between planes of given Miller indices h, k, and l.

In the hexagonal structure of ZnO, the plane spacing is related to the lattice constant a and the Miller indices by the following relation[37]

$$\frac{1}{d_{(hkl)}^2} = \frac{4}{3}\left(\frac{h^2 + hk + k^2}{a^2}\right) + \frac{l^2}{c^2} \tag{3}$$

with the first-order approximation, $n = 1$

$$\sin^2\theta = \frac{\lambda^2}{4a^2}\left[\frac{4}{3}(h^2 + k^2 + hk) + \left(\frac{a}{c}\right)^2 l^2\right] \tag{4}$$

For the (100) orientation at $2\theta = 31.79°$, the lattice constant a was calculated by

$$a = \frac{\lambda}{\sqrt{3}\sin\theta} \tag{5}$$

and for the (002) orientation at $2\theta = 34.42°$, the lattice constant c was calculated by

$$c = \frac{\lambda}{\sin\theta} \tag{6}$$

The lattice constants a and c were determined as $a = 3.249$ Å and $c = 5.206$ Å for pure ZnO.[31]

For Sb-doped ZnO, an increase in the lattice parameters a and c (3.261 and 5.228 Å, respectively) would be expected when Zn^{2+} ions are replaced by Sb^{3+} ions due to mismatch in ionic radii. Another possibility for the increase in the lattice parameters could be the formation of electrically inactive $Sb_{Zn}-Sb_i$ pairs described by Wardle et al.[38]

Ag-doping further increased both "a" and "c" parameters of the ZnO wurtzite structure. An increase in the lattice parameters a and c to 3.270 and 5.239 Å, respectively, has been determined when Zn^{2+} ions are replaced by Ag^{1+} ions because of the larger radius of Ag^+ ions (0.126 nm) than Zn^{2+} ions (0.074 nm). The increase in the lattice parameters could be caused by either interstitial incorporation of Ag ions into the lattice or Ag ion
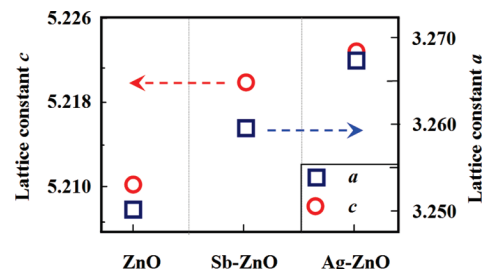

Figure 4. Lattice constants of pure and Sb- and Ag-doped ZnO nanorods on Si substrates. Unit of the lattice constants is Å.

substitution of the Zn ion.[35] The observed lattice constants a and c for Sb-doped and Ag-doped ZnO nanorods are presented in Figure 4.

Using energy dispersion X-ray spectroscopy (EDX), the Zn:O ratio in our nanostructures was analyzed and found to be 1:1 atomic ratio in pure samples. Nevertheless, since EDX cannot distinguish O in ZnO, ZnO_x, CO, and CO_2 (adventitious), the previously obtained ratio indicates an oxygen deficiency in the ZnO nanostructures since it also took into consideration O species not bound to Zn. A more quantitative estimation of the Zn:O ratios can be obtained by XPS since the different oxygen species can be deconvoluted from the O-1s binding energy region, and only O in ZnO and ZnO_x is used in the calculation of the Zn:O ratio. As will be discussed later in the XPS section, our nanostructures were found to be oxygen deficient. The EDX spectra of these samples indicate that the positions of the peaks O-K_α, Zn-L_α, and Ag-L_α appeared at 0.817, 1.109, and 2.983 keV, respectively. The quality of the grown ZnO rods is demonstrated by the stoichiometric composition deduced from the EDX analysis as well as by the XRD crystallographic data. Antimony or silver content in zinc oxide nanorods was found to be about 5% and 3% for samples #2 and #3, respectively.

3.2. Micro Raman Scattering. Raman scattering is sensitive to crystallization, structural disorder, and defects in micro- and nanostructures. It permits investigations on the local structure and vibrational modes in Ag- and Sb-doped ZnO nanorods. There is a number of detailed studies of the Raman active modes and the lattice dynamics of bulk ZnO.[44,46,48,50] Recently, Raman spectra of ZnO films doped with N, Fe, Sb, Al, Ga, Co, Mn, and Ag were reported by different groups.[39–42] Additional/local vibrational modes (LVMs) were found, such as the mode at 411 cm^{-1} for Ag doped, at 531 cm^{-1} for Sb doped, at 631 cm^{-1} for Ga doped, at 638 cm^{-1} for Ni doped, and at 720 cm^{-1} for Fe doped ZnO thin films.[39,42,51–60] The origin of these modes is arguable, and Manjon et al.[43] attributed the additional or local vibrational modes to the breakdown of the translation symmetry of the lattice caused by defects or impurities.

We have measured micro-Raman spectra of the pure and doped-ZnO nanorods to investigate whether there are large influences of Ag and Sb doping on the Raman spectra of zinc oxide nanorods. ZnO with a wurtzite structure belongs to the C_{6v}^4 (P6$_3$mc) space group, and there are 12 degrees of freedom since there are 4 atoms per primitive cell. Therefore, there are 9 optical phonon modes and 3 acoustic phonon modes, namely, three longitudinal-optical (LO) and six transverse-optical (TO) branches, one longitudinal-acoustic (LA), and two transverse-acoustic (TA). The different symmetries involved govern whether vibrations are Raman active and appear in the spectra, while changes in lattice spacing and chemical environment may shift the vibrational frequencies. Group theory predicts the optical phonons at the Γ point of the Brillouin zone, which have the representation[44]

Characterization of Ag- or Sb-Doped ZnO Nanorods

J. Phys. Chem. C, Vol. 114, No. 29, 2010 **12405**

$$\Gamma_{opt} = 1A_1 + 1E_1 + 2E_2 + 2B_1 \qquad (7)$$

where A_1, E_1, and E_2 modes are Raman active phonons and A_1 and E_1 are also infrared active.[44] The polar characteristics of the A_1 and E_1 modes are split into longitudinal (LO) and transverse optical (TO) components due to the macroscopic electric fields associated with the LO phonons.[44] Phonon modes of A_1 (574 and 380 cm^{-1}), E_1 (583 and 407 cm^{-1}), and E_2 (101 and 437 cm^{-1}) modes are Raman active, and the B_1 mode is silent at Raman spectra.[45,48,50] B_1 (low) and B_1 (high) modes are normally silent and are Raman inactive phonons.

Micro-Raman spectra of the pure and doped-ZnO nanorods are shown in Figure 5. These measurements were performed at room temperature over the frequency range from 60 to 900 cm^{-1}. Dominant peaks at 101 and 439 cm^{-1} (see Figure 5), which are commonly detected in the wurtzite structure ZnO,[44,48,50] are attributed to the low- and high-E_2 mode (E_2^L and E_2^H) of nonpolar optical phonons. The Raman bands at 383 and 416 cm^{-1} (Ag$-$ZnO) reflecting the strength of the polar lattice bonds are assigned to the A_1(TO) mode and E_1(TO) modes, respectively. A smaller peak at 334 cm^{-1} is attributed to a $E_2^H-E_2^L$ (multiphonon) mode.[50] The frequencies of the observed Raman bands are summarized in Table 2 and compared with the Raman band obtained for a bulk ZnO crystal given by Calleja and Cardona.[48] These peaks have been assigned to the second-order Raman spectrum arising from zone-boundary (M point) phonons 2-TA(M), 2-E_2(M), and 2-LA(M), respectively.[50] However, the coupling to plasmons in highly doped material and stress-induced effects due to lattice mismatch with the substrate might play a role in the interpretation of the observed phonon frequencies.[49] Within the spectral resolution of 2 cm^{-1}, there are no discernible frequency shifts between the ZnO and the doped nanorods. In the Sb-doped nanorods, a broadening of the bands due to the low-E_2 and high-E_2 modes may suggest larger lattice distortion due to the dopant.

Nanorods produced by chemical methods normally have more defects than corresponding bulk crystals. The A_1(LO) phonon band becomes stronger only in the sample with higher crystallinity. Influence of defects on the 574 cm^{-1} mode has been discussed.[47,59] The peak at 532 cm^{-1} in the Sb doped sample may be due to a 2LA vibration.[50] The intense peak near 441 cm^{-1} due to the E_2^H mode displays a clear asymmetry toward low frequencies. The asymmetric line shape has been analyzed in detail by Cusco et al.[50] It could be successfully explained in terms of resonant anharmonic interaction of the E_2^H mode with a band of combined transverse and longitudinal acoustic modes, as the steep variation of the two-phonon density of states around the E_2^H frequency leads to a distorted phonon line shape.

3.3. Chemical Characterization (XPS). XPS was used to characterize the composition of the following nanorod samples: pure ZnO (sample #1), Sb-doped ZnO (sample #2), and Ag-doped ZnO (sample #3). Positive binding energy (BE) shifts were observed in the XPS spectra due to charging effects. Therefore, the BE scale was calibrated using the adventitious carbon peak (C-1s) at 285 eV as reference.[47,61] In our samples, residual amounts of adventitious carbon and carbonyl compounds are unavoidable due to their exposure to air prior to the XPS analysis.[62] In addition to the adventitious carbon peak, the C-1s XPS spectrum of our samples (not shown) also shows two additional peaks at 286.6 and 288.7 eV corresponding to CO and CO_2, respectively.[62-64] As will be described below, those peaks were also used as a reference in the determination of the different O species present in our samples.

Figure 6 shows XPS spectra of the core level regions of (a) Zn-2p, (b) Sb-4d, and (c) Ag-3d. The undoped ZnO nanorods
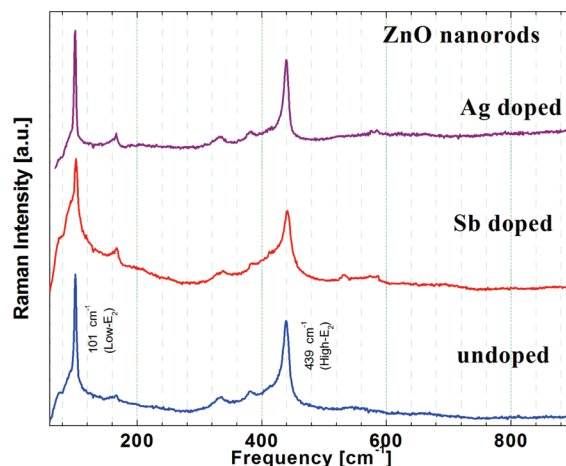
Figure 5. Micro-Raman scattering spectra of the pure ZnO nanorods, Sb-doped ZnO nanorods, and Ag-doped ZnO nanorods. Excitation wavelength is 633 nm.

TABLE 2: Experimental Values for Frequencies (cm^{-1}) of the Active Modes of Pure and Sb- and Ag-Doped-ZnO Nanorods and ZnO Crystal at Room Temperature

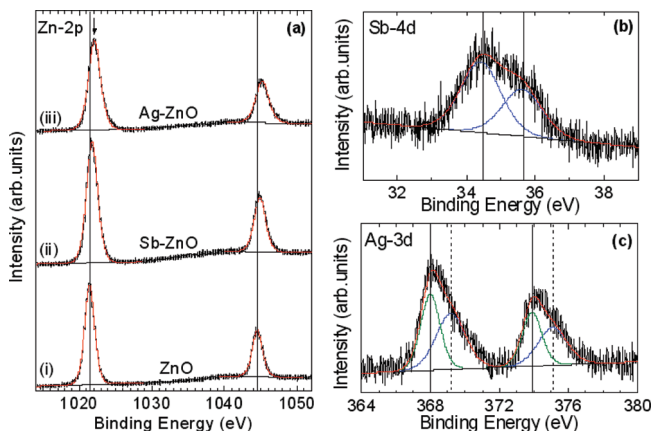| mode	ZnO nanorods, our results (cm^{-1})	Sb$-$ZnO nanorods, our results (cm^{-1})	Ag$-$ZnO nanorods, our results (cm^{-1})	ZnO crystal (cm^{-1})[a]
E_2^L	101	102	101	101
E_2^H	439	441	439	437
A_1(TO)	382	383	383	380
E_1(TO)			416	408
A_1(LO)	574	574	574	574
E_1(LO)		587	584	584

[a] Ref 48.

Figure 6. XPS spectra (Al Kα = 1486.6 eV) corresponding to the (a) Zn-2p, (b) Ag-3d, and (c) Sb-4d core levels of (i) pure ZnO nanorods and (ii) Sb- and (iii) Ag-doped ZnO nanorods supported on SiO$_2$/Si(001).

(sample #1) display a doublet at 1021.4 and 1044.5 eV (vertical reference lines) corresponding to the Zn-2p$_{3/2}$ and 2p$_{1/2}$ core levels.[65,66] However, when the ZnO nanorods were doped with Sb (sample #2) or Ag (sample #3), the Zn-2p levels were found to be shifted to higher binding energies. BE shifts of +0.4 eV for Sb$-$ZnO and +0.7 eV for Ag$-$ZnO were measured with respect to similarly sized pure ZnO nanorods. Similar trends (+0.7 eV shifts) were reported by Shin et al.[67] while comparing the Zn-2p$_{3/2}$ BEs of undoped and doped-ZnO (Ag, Li, and Al). The fwhm values of the Zn-2p peaks were also found to be larger for the Sb-doped (1.8 eV) and Ag-doped (1.9 eV) samples as compared to the pure ZnO (1.6 eV) nanorods. Since the size

TABLE 3: Summary of XPS Results Obtained on Pure and Ag- and Sb-Doped ZnO Nanorods[a]

			XPS binding energy (eV) [fwhm]			
sample	description	compounds	Zn-2p$_{3/2}$	Sb-4d$_{5/2}$	Ag-3d$_{5/2}$	dopant/ZnO
#1	ZnO	ZnO	1021.4 [1.6]			
#2	Sb−ZnO	ZnO	1021.8 [1.8]			Sb/Zn = 5%
		Sb$_2$O$_5$ or Sb−O−Zn		34.4 [1.4]		
#3	Ag−ZnO	ZnO	1022.1 [1.9]			Ag/Zn = 3%
		Ag^0 or Ag$_2$O			368 [1.3]	
		Ag−Zn−O			369.2 [2.0]	

[a] Included are the binding energies of different components (ZnO, Sb$_2$O$_5$, Ag$_2$O, and Ag^0) as well as the atomic percentage ratios of the dopants introduced in ZnO. The fwhm values are indicated between brackets.
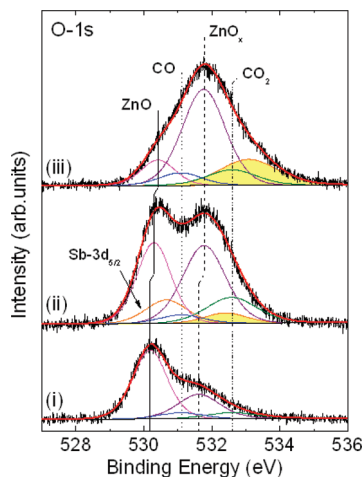

Figure 7. XPS spectra (Al Kα = 1486.6 eV) corresponding to the O-1s core level of (i) pure ZnO and (ii) Sb- and (iii) Ag-doped ZnO nanorods supported on SiO$_2$/Si(001).

of the ZnO nanorods was similar in all three samples, the broadening of the Zn-2p XPS peaks suggests the presence of additional chemical states of Zn, indicating the possible formation of Sb−Zn−O and Ag−Zn−O bonds.[68] Table 3 summarizes the results of the XPS analysis.

The Sb-4d and Ag-3d XPS binding energy regions of samples #2 and #3 are shown in Figures 6(b) and (c), respectively. The Sb-4d region of sample #2 was fitted with a doublet (34.4 eV, 35.6 eV, solid lines) corresponding to the Sb-4$_{5/2}$ and 4d$_{3/2}$ core levels of either Sb$_2$O$_5$ or Sb−O−Zn.[69] The Ag-3d BE region [Figure 6(c)] consists of an asymmetric peak that could be fitted with two doublets tentatively assigned to the Ag-3d$_{5/2}$ and 3d$_{3/2}$ core levels of two different species: (i) metallic Ag[69,70] or Ag$_2$O[71] (Ag-3d$_{5/2}$ = 368 eV, 52% of the total Ag XPS signal, solid line) and (ii) a Ag−Zn−O ternary compound (Ag-3d$_{5/2}$ = 369.2 eV, 48%, dashed line). An assignment of the first doublet to metallic Ag would be in agreement with Zhao et al.,[68] who reported a 368.2 eV BE for Ag-3d$_{5/2}$ in Ag-doped ZnO. Interestingly, their SEM data indicated the formation of Ag clusters on their samples. Duan et al.[71] showed similar clustering of the Ag dopants in ZnO however, their 367.8 eV Ag-3d$_{5/2}$ BE was assigned to Ag$_2$O. Due to the complexity of the O-1s region of sample #3 (see below), we cannot unambiguously assign the first doublet observed in the Ag-3d BE region to either metallic Ag or Ag$_2$O. From the XPS intensity (integrated area) ratios (Ag-3d/Zn-2p and Sb-4d/Zn-2p), Ag dopings of ∼3 atom % and ∼5 atom % Sb were determined after proper normalization by the corresponding atomic sensitivity factors (ASF).

The asymmetric peaks observed in the O-1s region (Figure 7) were deconvoluted by several subspectral components: (i) ZnO (530.2 eV), (ii) defective ZnO$_x$ or ZnOH (531.6 eV), (iii) Sb$_2$O$_5$ or Sb−O−Zn (sample #2, 532.4 eV), (iv) Ag$_2$O or

Ag−O−Zn or adsorbed oxygen species (sample #3, 533.1 eV), (v) adventitious CO (531.1 eV, dotted line),[72] and (vi) adventitious CO$_2$ (532.5 eV, dashed-dotted line).[73,74]

In addition to small CO and CO$_2$ signals, the undoped ZnO sample (sample #1) [Figure 7(i)] shows two peaks at 530.2 eV (solid line) and 531.6 eV (dashed line) that were assigned to O^{2-} ions in stoichiometric Zn−O−Zn and to an oxygen-deficient ZnO$_x$ region, respectively.[75−77] Armelao et al.[78] and Liqiang et al.[70] observed similar components in their O-1s spectra and attributed the high BE state to Zn−OH species. Considering their O-1s/Zn-2p XPS intensity ratios, the ZnO$_x$(OH)$_y$ stoichiometry was suggested.[78] In our studies, the O-1s/Zn-2p ratio was found to be 1.3 ± 0.1. Thus, the 531.6 eV component could be attributed to the presence of ZnO$_x$[75−77] or ZnOH.[70,78]

Besides the four components described above, the O-1s region of the Sb-doped ZnO (sample #2) [Figure 7(ii)] also contains a convoluted Sb-3d$_{5/2}$ peak at 530.7 eV (the other Sb-3d$_{3/2}$ spin−orbit pair peak is not shown here since it appears at 540 eV), as well as an O-1s from Sb$_2$O$_5$ at 532.4 eV (shaded peak). The O-1s/Sb-4d peak intensities (normalized by the ASF) were found to be 2.6, confirming the Sb$_2$O$_5$ stoichiometry.

The O-1s BE region of the Ag-doped ZnO (sample #3) [Figure 7(iii)] displays a broad peak fitted with subspectra corresponding to stoichiometric and defective ZnO (or ZnOH compounds), CO, and CO$_2$ and an additional feature at 533.1 eV (shaded peak) not present in the other samples. This feature could be assigned to Ag$_2$O species. However, since the O-1s/Ag-3d peak intensity ratio was found to be 5.6 and the BE measured is higher than the values reported in the literature for O in Ag-oxides,[65] this component has been tentatively attributed to adsorbed oxygen species (i.e., H$_2$O or adsorbed O$_2$).[77,79] It should, however, be noted that the presence of Ag$_2$O [in agreement to our Ag-3d data from Figure 6(c)] cannot be discarded since size effects could lead to a positive shift in the BE observed for this compound.

Our XPS data on the undoped ZnO (sample #1) indicate the existence of a lower concentration of defective ZnO$_x$ or ZnO$_x$(OH)$_y$ as compared to stoichiometric ZnO [ZnO$_x$ and/or ZnO$_x$(OH)$_y$/ZnO = 0.5] [Figure 7(i)]. However, when the dopants are introduced, the intensity of the nonstoichiometric ZnO$_x$ and/or ZnO$_x$(OH)$_y$ component increases, suggesting that the dopants might be substituting interstitial zinc vacancies (Sb− or Ag−O−Zn).[67,68,70] It is well-known that defects in ZnO film are formed by oxygen vacancies, zinc vacancies, interstitial zinc, interstitial oxygen, and antisite oxygen.[68] Thus, ternary compounds with Sb or Ag occupying the oxygen and zinc vacancies are expected, which is in accordance with our XRD and Raman data. Analysis of the intensity ratios of ZnO$_x$ and/or ZnO$_x$(OH)$_y$/ZnO leads to 1.2 in Sb−ZnO (sample #2) and 4.7 in Ag−ZnO (sample #3). This represents a total content of stoichiometric ZnO of 45% and 18% in samples #2 and #3, respectively. In contrast, a significantly higher content of stoichiometric ZnO

Characterization of Ag- or Sb-Doped ZnO Nanorods

J. Phys. Chem. C, Vol. 114, No. 29, 2010 **12407**

(67%) was obtained for the analogously prepared undoped ZnO sample. For the Ag−ZnO sample, this ratio could be attributed to the increased number of Ag atoms occupying O sites, while the Sb atoms seem to most likely occupy Zn sites.[80] The latter is in agreement with first-principles calculations by Limpijumnong et al.,[15] indicating that $Sb_{Zn}-2V_{Zn}$ complexes (V represents Zn vacancies) with 4-fold Sb coordination had the lowest formation energy. Previous studies on Ag-doped ZnO have suggested that Ag acts as an amphoteric dopant; i.e., Ag can be present in substitutional Zn sites as well as in interstitial sites.[26] However, first-principle calculations by Yan et al.[81] showed that substitutional sites are more energetically favorable than interstitial sites. In our studies, the second doublet observed in the Ag region [Figure 6(c)] suggests the formation of Ag−Zn bonds.[82]

4. Conclusion

In summary, pure and Sb- and Ag-doped ZnO nanorods were successfully synthesized through a facile hydrothermal route without the use of catalysts, templates, and seeds. ZnO nanorods are found to have high crystal quality. Each individual ZnO rod showed a hexagonal basis.

X-ray diffraction, scanning electron microscopy, X-ray photoelectron spectroscopy, and micro-Raman spectroscopy have been used to characterize the structure, morphology, and chemical composition of the samples. The ZnO rods synthesized were found to be of single-crystal quality with hexagonal wurtzite structure and stoichiometric ZnO composition. XRD measurements indicate that the synthesized ZnO crystals are in the hexagonal phase and well-aligned parallel to the [0001] crystal direction.

From XRD, results have been calculated for lattice constants *a* and *c* for Ag-doped ZnO nanorods. With the doping concentration of 3%, the lattice constant *a* increases from 3.250 to 3.270 Å, and *c* increases from 5.210 to 5.239 Å. Micro-Raman measurements provide further evidence that the pure and doped ZnO nanorods have a wurtzite structure.

Our XPS measurements demonstrated the presence of Sb and Ag in our samples. Furthermore, Sb_2O_5 or Sb−O−Zn[69] were found to be the most likely compounds on the Sb-doped ZnO nanorods. Analysis from the Ag XPS spectra revealed the presence of two different components that were attributed to either metallic Ag[68,70] or Ag_2O[71] and to a Ag−Zn−O ternary compound.

SEM images show that the nanorods' growth can be completed in 20 min and regulated by growth parameters. The main advantage of the proposed synthesis is its simplicity, low temperature (95 °C), and fast growth rates. Further work on the optimization of pure and doped ZnO nanorod growth for electronic and optoelectronic device applications is in progress. It is anticipated that the ZnO nanorods will find many applications[1,6,83−86] in novel nanodevices.

References and Notes

(1) Lupan, O.; Chow, L.; Chai, G.; Chernyak, L.; Lopatiuk-Tirpak, O.; Heinrich, H. *Phys. Status Solidi* **2008**, *205*, 2673.

(2) Lupan, O.; Chai, G.; Chow, L. *Technical Proceedings of the 2008 NSTI Nanotechnology Conference and Trade Show, NSTI-Nanotech, Nanotechnology*; June 1−5, 2008, Boston, Massachusetts, Vol. 3, pp 5−8.

(3) Lee, S. D.; Kim, Y. S.; Yi, M. S.; Choi, J. Y.; Kim, S. W. *J. Phys. Chem. C* **2009**, *113* (20), 8954.

(4) (a) Lupan, O.; Pauporté, Th.; Viana, B. Low-Voltage UV-Electroluminescence from ZnO-Nanowire Array/p-GaN Light-Emitting Diodes. *Adv. Mat.* **2010**, DOI: 10.1002/adma.201000611. (b) Fang, X.; Li, J.; Zhao, D.; Shen, D.; Li, B.; Wang, X. *J. Phys. Chem. C* **2009**, *113* (50), 21208. (c) Chen, C. H.; Chang, S. J.; Chang, S. P.; Li, M. J.; Chen, I. C.; Hsueh, T. J.; Hsu, C. L. *Appl. Phys. Lett.* **2009**, *95*, 223101.

(5) Ohno, Y.; Shirahama, T.; Takeda, S.; Ishizumi, A.; Kanemitsu, Y. *Appl. Phys. Lett.* **2005**, *87*, 043106.

(6) Lupan, O.; Chai, G.; Chow, L. *Microelectron. J.* **2007**, *38*, 1211.

(7) Lupan, O.; Ursaki, V. V.; Chai, G.; Chow, L.; Emelchenko, G. A.; Tiginyanu, I. M.; Gruzintsev, A. N.; Redkin, A. N. *Sens. Actuators, B* **2010**, *144*, 56.

(8) Zhang, S. B.; Wei, S. H.; Zunger, A. *Phys. Rev. B* **2001**, *63*, 075205.

(9) Egelhaaf, H. J.; Oelkrug, D. *J. Cryst. Growth* **1996**, *161*, 190.

(10) Gulino, A.; Fragala, I. *Chem. Mater.* **2002**, *14*, 116.

(11) Kim, K. K.; Kim, H. S.; Hwang, D. K.; Lim, J. H.; Park, S. J. *Appl. Phys. Lett.* **2003**, *83*, 63.

(12) Gao, K. Y.; Seyller, T.; Ley, L.; Ciobanu, F.; Pensl, G.; Tadich, A.; Riley, J. D.; Leckey, R. G. C. *Appl. Phys. Lett.* **2003**, *83*, 1830.

(13) Look, D. C.; Renlund, G. M.; Burgener, R. H.; Sizelove, J. R. *Appl. Phys. Lett.* **2004**, *85*, 5269.

(14) Zeng, Y. J.; Ye, Z. Z.; Xu, W. Z.; Li, D. Y.; Lu, J. G.; Zhu, L. P.; Zhao, B. H. *Appl. Phys. Lett.* **2006**, *88*, 062107.

(15) Limpijumnong, S.; Zhang, S. B.; Wei, S. H.; Park, C. H. *Phys. Rev. Lett.* **2004**, *92*, 155504.

(16) Pan, X.; Ye, Z.; Li, J.; Gu, X.; Zeng, Y.; He, H.; Zhu, L.; Che, Y. *Appl. Surf. Sci.* **2007**, *253*, 5067.

(17) Xiu, F. X.; Yang, Z.; Mandalapu, L. J.; Zhao, D. T.; Liu, J. L.; Beyermann, W. P. *Appl. Phys. Lett.* **2005**, *87*, 152101.

(18) Xiu, F. X.; Yang, Z.; Mandalapu, L. J.; Zhao, D. T.; Liu, J. L. *Appl. Phys. Lett.* **2005**, *87*, 252102.

(19) Kang, H. S.; Ahn, B. D.; Kim, J. H.; Kim, G. H.; Lim, S. H.; Chang, H. W.; Lee, S. Y. *Appl. Phys. Lett.* **2006**, *88*, 202108.

(20) Kim, I. S.; Jeong, E. K.; Kim, D. Y.; Kumar, M.; Choi, S. Y. *Appl. Surf. Sci.* **2009**, *255*, 4011.

(21) Yan, Y. F.; Wei, S. H. *Phys. Status Solidi B* **2008**, *245*, 641.

(22) Look, D. C. *Semicond. Sci. Technol.* **2005**, *20*, s55.

(23) Strikant, V.; Clark, D. R. *J. Mater. Res.* **1997**, *12*, 1425.

(24) Sun, M.; Zhang, Q.-F.; Wu, J.-L. *J. Phys. D: Appl. Phys.* **2007**, *20*, 3798.

(25) Galvan, A. M.; Cruz, C. T.; Lee, J.; Bhattacharyya, D.; Metson, J. *J. Appl. Phys.* **2006**, *99*, 014306.

(26) Ahn, B. D.; Kang, H. S.; Kim, J. H.; Kim, G. H.; Chang, H. W.; Lee, S. Y. *J. Appl. Phys.* **2006**, *100*, 093701.

(27) Sahu, D. R. *Microelectron. J.* **2007**, *38*, 1252.

(28) Chu, S.; Lim, J. H.; Mandalapu, L. J.; Yang, Z.; Li, L.; Liu, J. L. *Appl. Phys. Lett.* **2008**, *92*, 152103.

(29) Shishiyanu, S. T.; Lupan, O. I.; Shishiyanu, T. S.; Şontea, V. P.; Railean, S. K. *Electrochim. Acta* **2004**, *49*, 4433.

(30) Lupan, O.; Chow, L.; Chai, G.; Schulte, A.; Park, S.; Heinrich, H. *Mater. Sci. Eng. B* **2009**, *157*, 101−104.

(31) American Society for Testing and Material. *Powder Diffraction Files*; Joint Committee on Powder Diffraction Standards: Swarthmore, PA, 1999, pp 3−888.

(32) Houng, B.; Huang, C. *Surf. Coat. Technol.* **2006**, *201*, 3188.

(33) *CRC Handbook of Chemistry and Physics*, 65th ed.; CRC: Boca Raton, FL, CRC/Taylor & Francis, 2006.

(34) Shannon, R. D. *Acta Crystallogr. A* **1976**, *32*, 751.

(35) (a) Gruzintsev, A. N.; Volkov, V. T.; Yakimov, E. E. *Semiconductors* **2003**, *37*, 275. (b) Zhang, Y.; Zhang, Z.; Lin, B.; Fu, Z.; Xu, J. *J. Phys. Chem. B* **2005**, *109*, 19200−19203.

(36) Jin, Z.; Murakami, M.; Fukumura, T.; Matsumoto, Y.; Ohtomo, A.; Kawasaki, M.; Koinuma, H. *J. Cryst. Growth* **2000**, *214*, 55.

(37) Cullity, B. D.; Stock, S. R. *Elements of X-Ray Diffraction*, 2nd ed.; Prentice Hall: NJ, 2001.

(38) Wardle, M. G.; Goss, J. P.; Briddon, P. R. *Phys. Rev. B* **2005**, *71*, 155205.

(39) Bundesmann, C.; Ashkenov, N.; Schubert, M.; Spemann, D.; Butz, T.; Kaidashev, E. M. *Appl. Phys. Lett.* **2003**, *83*, 1974.

(40) Kaschner, A.; Haboeck, U.; Strassburg, M.; Strassburg, M.; Kaczmarczyk, G.; Hoffmann, A.; Thomsen, C.; Zeuner, A.; Alves, H. R.; Hofmann, D. M.; Meyer, B. K. *Appl. Phys. Lett.* **2002**, *80*, 1909.

(41) Alaria, J.; Bouloudenine, M.; Schmerber, G.; Colis, S.; Dinia, A.; Turek, P.; Bernard, M. *J. Appl. Phys.* **2006**, *99*, M118.

(42) Wang, X. B.; Song, C.; Geng, K. W.; Zeng, F.; Pan, F. *J. Phys. D: Appl. Phys.* **2006**, *39*, 4992.

(43) Manjon, F. J.; Mari, B.; Serrano, J.; Romero, A. H. *J. Appl. Phys.* **2005**, *97*, 053516.

(44) Arguello, C. A.; Rousseau, D. L.; Porto, S. P. S. *Phys. Rev.* **1969**, *181*, 1351.

(45) Ashkenov, N.; Mbenkum, B. N.; Bundesmann, C.; Riede, V.; Lorenz, M.; Spemann, D.; Kaidashev, E. M.; Kasic, A.; Schubert, M.; Grundmann, M.; Wagner, G.; Neumann, H.; Darakcjieva, V.; Arwin, H.; Monemar, B. *J. Appl. Phys.* **2003**, *93*, 126.

(46) Lupan, O.; Pauporté, T.; Chow, L.; Viana, B.; Pellé, F.; Ono, L. K.; Roldan Cuenya, B.; Heinrich, H. *Appl. Surf. Sci.* **2010**, *256*, 1895–1907.

(47) Lupan, O.; Chow, L.; Chai, G.; Roldan Cuenya, B.; Naitabdi, A.; Schulte, A.; Heinrich, H. *Mater. Sci. Eng., B* **2007**, *145*, 57.

(48) Calleja, J. M.; Cardona, M. *Phys. Rev. B* **1977**, *16*, 3753.

(49) Ozgur, U.; Alivov, Y. I.; Liu, C.; Teke, A.; Reshchikov, M. A.; Dogan, S.; Avrutin, V.; Cho, S.-J.; Morkoc, H. *J. Appl. Phys.* **2005**, *98*, 041301.

(50) Cuscó, R.; Alarcón-Lladó, E.; Ibáñez, J.; Artús, L.; Jiménez, J.; Wang, B.; Callahan, M. J. *Phys. Rev. B* **2007**, *75*, 165202.

(51) Wang, F.; He, H.; Ye, Z.; Zhu, L.; Tang, H.; Zhang, Y. *J. Phys. D: Appl. Phys.* **2005**, *38*, 2919–2922.

(52) Tripathy, S.; Chua, S. J.; Chen, P.; Miao, Z. L. *J. Appl. Phys.* **2002**, *92*, 3503.

(53) Wang, X.; Li, Q.; Liu, Z.; Zhang, J.; Liu, Z.; Wang, R. *Appl. Phys. Lett.* **2004**, *84*, 4941.

(54) Cong, G. W.; Wei, H. Y.; Zhang, P. F.; Peng, W. Q.; Wu, J. J.; Liu, X. L.; Jiao, C. M.; Hu, W. G.; Zhu, Q. S.; Wang, Z. G. *Appl. Phys. Lett.* **2005**, *87*, 231903.

(55) Tak, Y.; Park, D.; Yong, K. *J. Vac. Sci. Technol. B* **2006**, *24* (4), 2047.

(56) Alim, K. A.; Fonoberov, V. A.; Balandin, A. A. *Appl. Phys. Lett.* **2005**, *86*, 053103.

(57) Richter, H.; Wang, Z. P.; Ley, L. *Solid State Commun.* **1981**, *39*, 625.

(58) Serrano, J.; Manjon, F. J.; Romero, A. H.; Widulle, F.; Lauck, R.; Cardona, M. *Phys. Rev. Lett.* **2003**, *90*, 055510.

(59) Vanheusden, K.; Warren, W. L.; Seager, C. H.; Tallant, D. R.; Voigt, J. A.; Gnade, B. E. *J. Appl. Phys.* **1996**, *79*, 7983.

(60) Weber, W. H.; Merlin, R. *Raman Scattering in Materials Science*; Springer: Berlin, 2000.

(61) Nefedov, V. I.; Salyn, Y. V.; Leonhardt, G.; Scheibe, R. *J. Electron Spectrosc. Relat. Phenom.* **1977**, *10*, 121.

(62) Kawase, K.; Tanimura, J.; Kurokawa, H.; Wakao, K.; Inone, M.; Umeda, H.; Teramoto, A. *J. Electrochem. Soc.* **2005**, *152*, G163.

(63) Joubert, O.; Pelletier, J.; Fiori, C.; Tan, T. A. N. *J. Appl. Phys.* **1990**, *67*, 4291.

(64) Salaneck, W. R.; Paton, A.; Clark, D. T. *J. Appl. Phys.* **1976**, *47*, 144.

(65) http://srdata.nist.gov/xps/.

(66) Strohmeier, B. R.; Hercules, D. M. *J. Catal.* **1984**, *86*, 266.

(67) Shin, M. H.; Park, M. S.; Jung, S. H.; Boo, J. H.; Lee, N. E. *Thin Solid Films* **2007**, *515*, 4950.

(68) Zhao, S. Q.; Zhou, Y. L.; Zhao, K.; Liu, Z.; Han, P.; Wang, S. F.; Xiang, W. F.; Chen, Z. H.; Lu, H. B.; Cheng, B. L.; Yang, G. Z. *Phys. B* **2006**, *373*, 154.

(69) Zeng, D. W.; Xie, C. S.; Zhu, B. L.; Song, W. L.; Wang, A. H. *Mater. Sci. Eng., B* **2003**, *104*, 68.

(70) Liqiang, J.; Dejun, W.; Baiqi, W.; Shudan, L.; Baifu, X.; Honggang, F.; Jiazhong, S. *J. Mol. Catal. A: Chem.* **2006**, *244*, 193.

(71) Duan, L.; Lin, B. X.; Zhang, W. Y.; Zhong, S.; Fu, Z. X. *Appl. Phys. Lett.* **2006**, *88*, 232110.

(72) Tanaka, K.; Miyahara, K.; Toyoshima, I. *J. Phys. Chem.* **1984**, *88*, 3504.

(73) Carley, A. F.; Hawkins, G.; Read, S.; Roberts, M. W. *Top. Catal.* **1999**, *8*, 243.

(74) Onishi, H.; Egawa, C.; Aruga, T.; Iwasawa, Y. *Surf. Sci.* **1987**, *191*, 479.

(75) Tak, Y.; Park, D.; Yong, K. J. *J. Vac. Sci. Technol., B* **2006**, *24*, 2047.

(76) Yang, X. J.; Miao, X. Y.; Xu, X. L.; Xu, C. M.; Xu, J.; Liu, H. T. *Opt. Mater.* **2005**, *27*, 1602.

(77) Chen, M.; Wang, X.; Yu, Y. H.; Pei, Z. L.; Bai, X. D.; Sun, C.; Huang, R. F.; Wen, L. S. *Appl. Surf. Sci.* **2000**, *158*, 134.

(78) Armelao, L.; Fabrizio, M.; Gialanella, S.; Zordan, F. *Thin Solid Films* **2001**, *394*, 90.

(79) Wang, Z. G.; Zu, X. T.; Yang, S. Z.; Wang, L. M. *J. Mater. Sci.* **2006**, *41*, 3729.

(80) Harrington, R.; Miles, G. C.; West, A. R. *J. Eur. Ceram. Soc.* **2006**, *26*, 2307.

(81) Yan, Y. F.; Al-Jassim, M. M.; Wei, S. H. *Appl. Phys. Lett.* **2006**, *89*, 181912.

(82) Chaturvedi, S.; Rodriguez, J. A. *Surf. Sci.* **1998**, *401*, 282.

(83) Lupan, O.; Chai, G.; Chow, L. *Microelectron. Eng.* **2008**, *85* (11), 2220.

(84) Chai, G.; Lupan, O.; Chow, L.; Heinrich, H. *Sens. Actuators, A* **2009**, *150*, 184.

(85) Lupan, O.; Chai, G.; Chow, L. *Sens. Actuators, B* **2009**, *141*, 511.

(86) Lupan, O.; Guérin, V. M.; Tiginyanu, I. M.; Ursaki, V. V.; Chow, L.; Heinrich, H.; Pauporté, Th. *J. Photochem. Photobiol. A: Chemistry* **2010**, *211*, 65.